Analysis and Detection of Forced Oscillation in Power System

Hua Ye, *Member, IEEE*, Yutian Liu, *Senior Member, IEEE*, Peng Zhang, *Senior Member, IEEE*, and Zhengchun Du, *Member, IEEE*

***Abstract*—To mitigate forced oscillation and avoid confusion with modal oscillation, fundamentals of forced oscillation in multi-machine power system are investigated. First, the explicit formulation of the oscillation is formulated in terms of forced disturbances and system mode shapes. Then, forced oscillation amplitude, components and envelope are intensively studied. Consequently, measures for mitigating the oscillation are obtained. Forced oscillation can also be effectively detected and discriminated from modal oscillation by utilizing its uniqueness of components properties and envelope shapes. Study results of the 10-machine 39-bus New England test system and a real-life power system demonstrate the correctness of theoretical analyses and effectiveness of detection methods for forced oscillation.**

***Index Terms*—Beat frequency oscillation, eigen-analysis, envelope, Forced oscillation, low frequency oscillation, resonance.**

I. Introduction

BEYOND the well-known modal (or natural, free) oscillations that are excited by random load fluctuations and sudden network switchings [1], sustained forced oscillations can emerge when power system is perturbed by periodic disturbances at frequencies close or equal to natural frequencies of system modes [2], [3]. Such oscillations have been observed from the western North American Power System, US Western Electricity Coordinating Council system, and the Nordic power system [4]. Compared with modal oscillation, forced oscillation exhibits extremely higher amplitude and may cause catastrophic blackout, especially in the poorly damped operating condition. The origins of forced oscillation are sinusoidal in nature, including cyclic loads [5]–[8], electrical oscillations due to malfunction of power system stabilizer (PSS) [2] and mechanical oscillations of generator turbines [3], [9]. The causes of mechanical oscillations are complex and strongly related to thermal process. Specifically, the major contributors may include unsteady combustion of boiler [10], turbo-pressure pulsations [11], undesirable steam turbine valve discharge characteristics [12]–[14], etc. Besides, wind power may fluctuate periodically and becomes a potential forced oscillation source because of wind shear and tower shadow effects [15], [16] and vibration of floating offshore wind turbine [17]. Therefore, forced oscillation becomes not only an important issue of power system but also one concern of integrating wind energy into modern power grid.

Since forced oscillation is significantly different from modal oscillation in nature, sources and control strategies, it is essential to study its fundamentals and take unique countermeasures to mitigate it. In addition, the rationale behind the similar appearances of forced oscillation and undamped modal oscillation should be fully understood to avoid possible confusion. So far, forced oscillation is still an open problem in power system community and few literatures are established on its fundamentals. Methods for detection and frequency estimation of forced oscillations are proposed in [18]–[21]. A spectral approach is presented in [22] to distinguish forced and modal oscillations. In [23], interactions between forced oscillation and system mode in the context of resonance are studied by numerical simulations rather than theoretical analyses.

To fill the gap in understanding forced oscillation, this paper studies the fundamentals of forced oscillation in multi-machine power system. First, its explicit expression is derived by directly solving system state equation and formulated in terms of forced disturbances and system mode shapes. Based on the expression, amplitude, components and envelope of forced oscillation are then intensively analyzed. Consequently, measures for mitigating the oscillation are obtained. Besides, two methods based on uniqueness of components properties and envelope shapes respectively are presented for detection of forced oscillation.

The contributions of this paper are threefold. First, how system mode affects amplitude of forced oscillation is fully understood by formulating and analyzing its explicit expression. Second, a distinction between forced and modal oscillations is made by comparing their differences in component quantities, frequencies and damping ratios. It enables one to detect forced oscillation excited by multiple disturbance sources. Third, the envelope of forced oscillation is intensively investigated. The

Manuscript received October 8, 2015; revised January 24, 2016 and May 7, 2016; accepted June 12, 2016. Date of publication June 14, 2016; date of current version February 16, 2017. This work was supported in part by the Natural Science Foundation of China under Grant 51107073 and the Specialized Research Fund for the Doctoral Program of Higher Education of China under Grant 11001311038, and Young Scholars Program of Shandong University (YSPSDU). The work of P. Zhang was supported in part by the U.S. National Science Foundation under Grant CNS-1419076. Paper no. TPWRS-01410-2015.

H. Ye and Y. Liu are with the Key Laboratory of Power System Intelligent Dispatch and Control of Ministry of Education, Shandong University, Ji'nan 250061, China (e-mail: yehua@sdu.edu.cn; liuyt@sdu.edu.cn).

P. Zhang is with the Department of Electrical and Computer Engineering, University of Connecticut, Storrs, CT 06269 USA (e-mail: peng.zhang@uconn.edu).

Z. Du is with the Department of Electrical Engineering, Xi'an Jiaotong University, Xi'an 710049, China (e-mail: zcdu@xjtu.edu.cn).

Color versions of one or more of the figures in this paper are available online at http://ieeexplore.ieee.org.

Digital Object Identifier 10.1109/TPWRS.2016.2580710

resultant envelope shapes are desirable for detection of forced oscillation in the case of single forced disturbance by visual inspection.

The remainder of the paper is organized as follows. Section II derives the explicit formulation of forced oscillation. Its amplitude, components and envelope are analyzed in Sections III–V, respectively. Studies of forced oscillations in the 10-machine 39-bus New England test system and a practical power system are given in Sections VI and VII, respectively. Section VIII draws conclusions of this paper.

II. Explicit Formulation of Forced Oscillation

In this section, the core of this paper, i.e., explicit formulation of forced oscillation, is obtained by directly solving system state equation and reducing the resultant solution.

A. Power System State Equation

The power system model for small signal stability analysis can be formulated by a set of homogeneous differential and algebraic equations linearized around an operating point [24]:

$$\begin{bmatrix} \dot{\boldsymbol{x}} \\ \boldsymbol{0} \end{bmatrix} = \begin{bmatrix} \boldsymbol{J}_1 & \boldsymbol{J}_2 \\ \boldsymbol{J}_2 & \boldsymbol{J}_4 \end{bmatrix} \begin{bmatrix} \Delta\boldsymbol{x} \\ \Delta\boldsymbol{z} \end{bmatrix} \tag{1}$$

where $\boldsymbol{x} \in \mathbb{R}^{n\times 1}$ is the vector of system state variables, and $\boldsymbol{z}$ is the vector of algebraic variables. $\boldsymbol{J}_1$–$\boldsymbol{J}_4$ are sparse Jacobian matrices. The system state equation can be obtained from (1) by eliminating the vector of algebraic variables:

$$\Delta\dot{\boldsymbol{x}} = \left(\boldsymbol{J}_1 - \boldsymbol{J}_2\boldsymbol{J}_4^{-1}\boldsymbol{J}_3\right)\Delta\boldsymbol{x} = \boldsymbol{A}\Delta\boldsymbol{x} \tag{2}$$

where $\boldsymbol{A}$ is the system state matrix.

B. Solution of System State Equation

Physically, periodic and forced disturbances mean there exists a certain amount of disturbed mechanical or electromagnetic power imposed on generator shaft. Accordingly, the dynamics of the power system can be described by superimposing a non-homogeneous term on (2).

$$\begin{cases} \Delta\dot{\boldsymbol{x}}(t) = \boldsymbol{A}\Delta\boldsymbol{x}(t) + \boldsymbol{B}\boldsymbol{u}(t) \\ \Delta y(t) = \boldsymbol{C}\Delta\boldsymbol{x}(t) \end{cases} \tag{3}$$

where $\boldsymbol{B}$ and $\boldsymbol{u}(t)$ are identity input matrix and forced disturbance vector, respectively. The forced disturbances on m generators have the form of $u_l = \Delta P_l \sin(\omega_l t),\ l = 1,\ \ldots,\ m$. ΔP_l and ω_l are magnitude and frequency (in rad/s) of the lth disturbance, respectively. $\boldsymbol{C} = [c_1,\ \cdots, c_n]$ is an output vector and $\Delta y(t)$ is an observation of the resultant forced oscillation.

In mathematics, the solution of $\Delta\boldsymbol{x}(t)$ in (3) is given as a sum of two parts and shown in (4) [25]. Physically, the first summand $\Delta\boldsymbol{x}_1(t)$ is *zero-input response* of the system, viz., the well-known *modal oscillation*. While the second summand $\Delta\boldsymbol{x}_2(t)$ describes *zero-state response* of the system, viz., *forced oscillation*.

$$\begin{aligned} \Delta\boldsymbol{x}(t) =&\ \Delta\boldsymbol{x}_1(t) + \Delta\boldsymbol{x}_2(t) \\ =&\ e^{\boldsymbol{A}t}\Delta\boldsymbol{x}(0) + \int_0^t e^{-\boldsymbol{A}(\tau-t)}\boldsymbol{B}\boldsymbol{u}(\tau)\mathrm{d}\tau. \end{aligned} \tag{4}$$

Since only the force oscillation is of our interests in this paper, a zero initial state deviation $\Delta\boldsymbol{x}(0)$ is assumed in (4). Accordingly, only $\Delta\boldsymbol{x}_2(t)$ is presented in $\Delta\boldsymbol{x}(t)$.

In the following Sections II-C and II-D, $\Delta\boldsymbol{x}_2(t)$ is first expanded and then reduced by utilizing the eigen-analysis theory, leading to an explicit expression of forced oscillation.

C. Expansion of Forced Oscillation

$\Delta\boldsymbol{x}_2(t)$ can be reformulated as follows by substituting the eigen-decomposition $\boldsymbol{A} = \boldsymbol{\Phi}\boldsymbol{\Lambda}\boldsymbol{\Psi}$ into (4):

$$\Delta\boldsymbol{x}_2(t) = \boldsymbol{\Phi}\int_0^t e^{-\boldsymbol{\Lambda}(\tau-t)}\boldsymbol{\Psi}\boldsymbol{B}\boldsymbol{u}(\tau)\mathrm{d}\tau \tag{5}$$

where $\boldsymbol{\Lambda}$ is a diagonal matrix with the distinct conjugate complex eigenvalue pairs $(\lambda_r,\ \lambda_r^*)$, $r = 1,\ \ldots,\ q$, as diagonal elements. λ_r and λ_r^* are also termed electromechanical oscillation modes of the system. $\boldsymbol{\Phi} = [\boldsymbol{\phi}_1,\ \ldots,\ \boldsymbol{\phi}_q,\ \boldsymbol{\phi}_1^*,\ \ldots,\ \boldsymbol{\phi}_q^*]$ and $\boldsymbol{\Psi} = [\boldsymbol{\psi}_1^{\mathrm{T}},\ \ldots,\ \boldsymbol{\psi}_q^{\mathrm{T}},\ \boldsymbol{\psi}_1^{*\mathrm{T}}, \ldots, \boldsymbol{\psi}_q^{*\mathrm{T}}]^{\mathrm{T}}$ are the corresponding right and left eigenvector matrices.

Equation (5) is further expanded and expressed in terms of forced disturbances, system modes, and the associated left and right eigenvectors.

$$\begin{aligned} \Delta\boldsymbol{x}_2(t) =&\ \sum_{r=1}^{q}\sum_{l=1}^{m}\Delta P_l\Big[\phi_{ir}\psi_{rl}e^{\lambda_r t}\int_0^t e^{-\lambda_r\tau}\sin(\omega_l\tau)\mathrm{d}\tau \\ &+ \phi_{ir}^*\psi_{rl}^*e^{\lambda_r^* t}\int_0^t e^{-\lambda_r^*\tau}\sin(\omega_l\tau)\mathrm{d}\tau\Big] \\ =&\ \sum_{r=1}^{q}\sum_{l=1}^{m}\Delta P_l \\ &\times\left\{\frac{\phi_{ir}\psi_{rl}[(-\lambda_r\sin\omega_l t - \omega_l\cos\omega_l t) + \omega_l e^{\lambda_r t}]}{\lambda_r^2+\omega_l^2}\right. \\ &\left.+\ \frac{\phi_{ir}^*\psi_{rl}^*[(-\lambda_r^*\sin\omega_l t - \omega_l\cos\omega_l t) + \omega_l e^{\lambda_r^* t}]}{\lambda_r^{*2}+\omega_l^2}\right\} \\ =&\ \sum_{r=1}^{q}\sum_{l=1}^{m}\frac{\Delta P_l}{(\lambda_r^2+\omega_l^2)(\lambda_r^{*2}+\omega_l^2)} \\ &\times\{\big[(\lambda_r^{*2}+\omega_l^2)\phi_{ir}\psi_{rl}e^{\lambda_r t} + (\lambda_r^2+\omega_l^2)\phi_{ir}^*\psi_{rl}^*e^{\lambda_r^* t}\big]\omega_l - \\ &\big[(\lambda_r^{*2}+\omega_l^2)\phi_{ir}\psi_{rl} + (\lambda_r^2+\omega_l^2)\phi_{ir}^*\psi_{rl}^*\big]\omega_l\cos\omega_l t - \\ &\big[(\lambda_r^{*2}+\omega_l^2)\phi_{ir}\psi_{rl}\lambda_r + (\lambda_r^2+\omega_l^2)\phi_{ir}^*\psi_{rl}^*\lambda_r^*\big]\sin\omega_l t\ \} \end{aligned} \tag{6}$$

where ϕ_{ir} and ψ_{rl} are the ith and lth entry of the rth right and left eigenvectors, respectively. They can be rewritten as:

$$\phi_{ir} = |\phi_{ir}|\angle\gamma_{ir},\ \psi_{rl} = |\psi_{rl}|\angle\alpha_{rl}. \tag{7}$$

D. Explicit Expression of Forced Oscillation

To simplify $\Delta\boldsymbol{x}_2(t)$, the rth system mode λ_r is detailed as follows [26]:

$$\lambda_r = \sigma_r + \mathrm{j}\omega_{\mathrm{d}r} = -\zeta_r\omega_{\mathrm{n}r} + \mathrm{j}\sqrt{1-\zeta_r^2}\omega_{\mathrm{n}r} = \omega_{\mathrm{n}r}\angle\theta_r \tag{8}$$

where ζ_r, $\omega_{\mathrm{n}r}$, $\omega_{\mathrm{d}r}$ and θ_r are termed damping ratio, undamped natural frequency (in rad/s), damped natural frequency (in rad/s) and damping angle of the rth system mode, respectively.

By utilizing the notations defined in (7) and (8), $\Delta \boldsymbol{x}_2(t)$ can be greatly reduced and the explicit expression of forced oscillation $\Delta y(t)$ is accordingly obtained:

$$\begin{aligned}\Delta y(t) &= \boldsymbol{C}\Delta \boldsymbol{x}_2(t) \\ &= \sum_{i=1}^{n}\sum_{r=1}^{q}\sum_{l=1}^{m} Z\big[e^{-\zeta_r \omega_{\mathrm{n}r} t}\sin(\omega_{\mathrm{d}r} t + \gamma_{ir} + \alpha_{rl} - \varphi) \\ &\quad -\beta \sin(\omega_l t + \gamma_{ir} + \alpha_{rl} - \varphi)\big] \end{aligned} \tag{9}$$

where Z is the amplitude of forced oscillation, ν is called as amplification factor, φ is the phase shift between the forced oscillation $\Delta y(t)$ and the lth forced disturbance u_l,

$$Z = c_i|\phi_{ir}||\psi_{rl}|\Delta P_l \times \nu,\ \nu = \frac{2\omega_l}{\eta} \tag{10}$$

$$\varphi = \tan^{-1}\left(\frac{\omega_{\mathrm{n}r}^2 - \omega_l^2}{2\zeta_r \omega_{\mathrm{n}r}^2}\right) \tag{11}$$

$$\eta = \sqrt{(\omega_{\mathrm{n}r}^2 - \omega_l^2)^2 + 4\zeta_r^2 \omega_{\mathrm{n}r}^2 \omega_l^2} \tag{12}$$

$$\beta = \sqrt{1 + \left(\frac{\omega_{\mathrm{n}r}^2}{\omega_l^2} - 1\right)\cos^2(\gamma_{ir} + \alpha_{rl} - \varphi)}. \tag{13}$$

More explanation on Z expressed in (10) is given as follows. The first term $c_i|\phi_{ir}||\psi_{rl}|\Delta P_l$ is identical to the amplitude of modal oscillation [26], [27] under the same magnitude of state deviation of ΔP_l. In this sense, the remaining term ν in Z represents the ratio of the amplitude of forced oscillation relative to that of modal oscillation. The name *amplification factor* comes from the fact that ν is generally greater than 1.0.

In summary, the explicit expressions of forced oscillation as given in (9)–(13) are the core of this paper because they lay the basis of forced oscillation amplitude, components and envelope analyses, as elaborated in parallel Sections III-V.

III. Forced Oscillation Amplitude-Analysis and Mitigation

In this section, factors that affect the amplitude of forced oscillation are studied from the two terms of Z, i.e., $c_i|\phi_{ir}||\psi_{rl}|\Delta P_l$ and ν, as expressed in (10) and (12).

A. Effects of Observability / Controllability of System Mode

Essentially, the term $c_i|\phi_{ir}||\psi_{rl}|\Delta P_l$ in Z represents the observability and controllability of the rth system mode. On one hand, $c_i|\phi_{ir}|$ measures observability of the rth system mode from the state variable x_i. On the other hand, $|\psi_{rl}|\Delta P_l$ weighs controllability (i.e., excitability) of the rth system mode by the lth forced disturbance. Therefore, large magnitudes of c_i and ΔP_l as well as high participating factor $|\phi_{ir}||\psi_{rl}|$ denote good observability and strong controllability. Accordingly, they will lead to remarkable amplitude of forced oscillation Z.

In practical power system, generators that strongly relate to a weakly damped inter-area mode always have high participating factors. If they are excited by injecting sustained and sinusoidal disturbances with large magnitudes, strong forced oscillations will emerge and can be easily captured at critical locations, e.g., tie-lines.

B. Effects of Frequency of Forced Disturbance and Damping Ratio of System Mode

The impacts of frequency proximity of ω_l to $\omega_{\mathrm{n}r}$ and damping ratio of the rth system mode ζ_r on forced oscillation amplitude Z are studied from η as expressed in (12).

To characterize the quantitative relationship between the two terms under the square root sign of η, an index called Forced Oscillation Ratio (FOR) is defined by using their ratios, i.e.,

$$\begin{aligned}\mathrm{FOR} &= \frac{(\omega_{\mathrm{n}r}^2 - \omega_l^2)^2}{4\zeta_r^2\omega_{\mathrm{n}r}^2\omega_l^2} = \frac{(\omega_{\mathrm{n}r} + \omega_l)^2(\omega_{\mathrm{n}r} - \omega_l)^2}{4\zeta_r^2\omega_{\mathrm{n}r}^2\omega_l^2} \\ &\approx \left[\frac{\omega_{\mathrm{n}r} - \omega_l}{\omega_{\mathrm{n}r}} \Big/ \zeta_r\right]^2 \approx \left[\frac{\omega_{\mathrm{n}r} - \omega_l}{\omega_l} \Big/ \zeta_r\right]^2 \geq 0. \end{aligned} \tag{14}$$

The physical meaning of FOR is square of the ratio of relative frequency difference between the lth disturbance ω_l and the rth system mode $\omega_{\mathrm{n}r}$, i.e., $\frac{\omega_{\mathrm{n}r} - \omega_l}{\omega_l}$ or $\frac{\omega_{\mathrm{n}r} - \omega_l}{\omega_{\mathrm{n}r}}$, to damping ratio of the rth system mode ζ_r.

With the help of FOR, the following statements can be made.

1) $FOR \gg 1$: This case denotes that the first item, i.e., $(\omega_{\mathrm{n}r}^2 - \omega_l^2)^2$, dominates the expression under the square root sign of η. Therefore, closer proximity of ω_l and $\omega_{\mathrm{n}r}$ will result in smaller η and hence greater ν.

2) $FOR \ll 1$: In this case, the square-product $4\zeta_r^2\omega_{\mathrm{n}r}^2\omega_l^2$ dominates the expression under the square root sign of η. Thus, it can be concluded that smaller ζ_r will also lead to smaller η and greater ν. Actually, this statement can also be made by further analyzing $4\zeta_r^2\omega_{\mathrm{n}r}^2\omega_l^2$.

First, identical to modal oscillation, forced oscillation occurs when power system is in weakly damping condition, $\zeta_r < 3\%$. Accordingly, we have $\zeta_r^2 < 9 \times 10^{-4}$. Second, as we know, both ω_l and $\omega_{\mathrm{n}r}$ fall into the low frequency interval $[0.628,\ 12.56]$ rad/s, then we get $\omega_{\mathrm{n}r}^2\omega_l^2 \in [0.3948,\ 157.9137]$. By qualitatively comparing the orders of magnitude of ζ_r^2 and $\omega_{\mathrm{n}r}^2\omega_l^2$, it is clear that it is ζ_r the most important determinant of $4\zeta_r^2\omega_{\mathrm{n}r}^2\omega_l^2$. Therefore, the same conclusion can be obtained as that derived from FOR: smaller ζ_r will also lead to smaller η and greater ν.

3) Otherwise: It can be seen from FOR that the two terms under the square root sign of η are comparable. That means that both the relative frequency difference $\frac{\omega_{\mathrm{n}r} - \omega_l}{\omega_l}$ (or $\frac{\omega_{\mathrm{n}r} - \omega_l}{\omega_{\mathrm{n}r}}$) and damping ratio of the rth system mode ζ_r will largely affect the amplitude of forced oscillation Z.

In summary, closer proximity of ω_l to $\omega_{\mathrm{n}r}$ in case $FOR \gg 1$ and smaller damping ratio of system mode ζ_r when $FOR \ll 1$ will result in smaller η and hence greater ν in Z.

C. Resonance and Beats

The maximums of ν and Z occur in the case of *resonance*. Mathematically, they can be obtained by taking derivatives of ν and Z with respect to ω_l and making them equal zero. It shows that the upper bounds of ν and Z are achieved when ω_l coincides

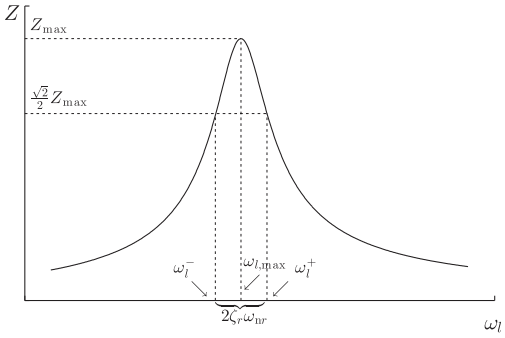

Fig. 1. Illustrative diagram of resonance curve, i.e., amplitude Z versus forced disturbance frequency ω_l, under a given damping ratio of ζ_r.

with ω_{nr}, i.e.,

$$\nu_{\max} = \frac{1}{\zeta_r \omega_{\mathrm{nr}}},$$
$$Z_{\max} = \frac{c_i |\phi_{ir}||\psi_{rl}|\Delta P_l}{\zeta_r \omega_{\mathrm{nr}}},\ \omega_{l,\max} = \omega_{\mathrm{nr}}. \tag{15}$$

At the resonant frequency $\omega_{l,\max}$, both $\nu_{\max}$ and $Z_{\max}$ decrease as ζ_r increases. Besides, under a given damping ratio ζ_r, ν and Z decay rapidly if ω_l goes far from $\omega_{l,\max}$. In particular, they decrease $\sqrt{2}$ times at two frequencies surrounding $\omega_{l,\max}$, as shown in Fig. 1.

$$\omega_l^{\pm} = \omega_{\mathrm{nr}} \sqrt{1 + 2\zeta_r^2 \pm 2\zeta_r \sqrt{1+\zeta_r^2}}. \tag{16}$$

The distance between ω_l^- and ω_l^+ is called *resonance peak width* (in frequency) and can be approximated as $2\zeta_r\omega_{\mathrm{nr}}$ [28]. Thus, the higher is the damping ratio ζ_r, the more is the resonance peak width.

If the frequency difference $|\omega_l - \omega_{l,\max}|$ exceeds half of the resonant peak width, i.e., $\zeta_r\omega_{\mathrm{nr}}$, but is still less than a threshold, the amplitude (envelope) of forced oscillation begins to oscillate. Accordingly, the forced oscillation becomes *beat frequency oscillation* or *beats* [29] for simplicity. The envelope shapes of both resonance and beats will be elaborated in Section V.

D. Measures for Mitigating Forced Oscillation

From Sections II-A to III-C, four theoretical measures can be straightforwardly derived for mitigating forced oscillation, i.e.,

1) to correct or disconnect the apparatus (i.e., disturbance sources) causing the oscillations,
2) to move the disturbance frequency ω_l far away from natural frequency of the system ω_{nr},
3) to reduce the amplitude of forced disturbance ΔP_l,
4) and to improve damping ratio of system mode ζ_r.

Generally speaking, measures 1) to 3) are unique for mitigating forced oscillation. While measure 4) suits for damping both forced and modal oscillations. In addition, it should be emphasized that measure 1) is the root approach to eliminate forced oscillation. While it can only be alleviated to some extent by measures 2) to 4) since forced disturbance source still drives the system.

Successful implementation of measures 1)–3) highly depends on two prerequisites: reliably locating forced disturbances to different ranges in advance, specifically, a region, a generator or even the control unit (i.e., governor, exciter and PSS) of a generator [30]–[33], and accurately detecting forced oscillation and discriminating it from modal oscillation. For the latter, two methods will be presented in Sections IV-B and V-D, respectively.

In the rest of this section, specific control strategies for mitigating forced oscillation are addressed in detail.

To implement the root measure 1), remedial actions should be taken to amend malfunctions of generator control units according to intensive post-fault analysis, so that desired control performances are regained. In extremely emergent state, as a final resort, measure 1) probably implies generator tripping or load shedding by system operators, which will result in major disturbances to power systems and consumers.

Practically, measures 2) and 4) are indirectly and implicitly realized by largely changing system operating conditions. Specifically, when the system is in emergency, forced oscillation can be alleviated by reducing the outputs of critical participating generators and/or upgrading their terminal voltage [34]. In this case, these operational actions are similar to those for modal oscillation [35].

Actually, measure 4) is the root approach to damp modal oscillation. Thus, the specific control strategies for improve system damping against forced and modal oscillation are identical. Specifically, they include reducing system loading and feedback controls, strengthening system structure, installing PSSs and other supplementary controllers on FACTS devices and HVDC systems.

IV. Forced Oscillation Components-Analysis and Detection

This section analyzes the components of forced oscillation. Based on uniqueness of component quantities, frequencies and damping ratios, a method is presented to detect the oscillation.

A. Oscillation Components Analysis

The transient response of forced oscillation contains twin components, corresponding to the two terms inside the square bracket of (9). One is termed as *forced component* of zero damping and with the same frequency as the forced disturbance. The other is called as *free (or natural) component*, whose oscillatory frequency and damping ratio are identical to those of system mode. In comparison, the well-known modal oscillation contains only one free component.

The free component dies out some time after the forced disturbance has been introduced. After that forced oscillation arrives in steady state and there leaves only the forced component. Therefore, if one wants to extract oscillatory properties of the system, data sampled at the initial stage of the forced oscillation is necessary where the free component is involved.

B. Component-Analysis-Based Forced Oscillation Detection

Both forced oscillation and system mode are supposed to be simultaneously and accurately estimated by certain modal

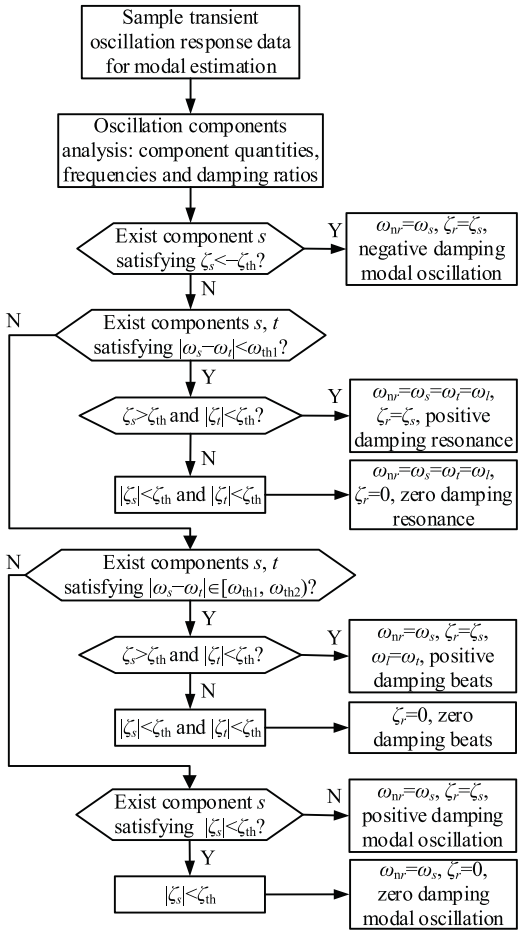

Fig. 2. Flowchart of component-analysis-based oscillation detection and discrimination.

estimation algorithm, such as stochastic subspace identification-covariance and Prony [36], [37].

Subsequently, forced oscillations (resonance and beats) and modal oscillation can be distinguished from each other according to differences in the estimated oscillation component quantities, frequencies and damping ratios. A flowchart for detecting and discriminating various oscillations is given in Fig. 2, including *positive/zero damping resonances, positive/zero damping beats, and negative/positive/zero damping modal oscillations*.

C. Determination of Damping Ratio and Frequency Thresholds

In Fig. 2, four additional symbols ω_s, ω_t, ζ_s, ζ_t are introduced to denote frequencies and damping ratios of two arbitrary estimated oscillation components s and t.

Considering there always exists some biased error in damping estimation, a relaxed inequality $|\zeta_s| < \zeta_{\rm th}$ is utilized to identify an oscillation component s of zero damping, where $\zeta_{\rm th}$ is chosen as a small positive number, e.g., 0.5%.

The thresholds $\omega_{\rm th1}$ and $\omega_{\rm th2}$ are employed to determine whether the two components s and t are two distinct components of a modal oscillation or twin components of a forced oscillation. Specifically,

1) if $|\omega_s - \omega_t|$ falls into the interval $[0,\ \omega_{\rm th1})$, components s and t are the twin components of resonance,
2) if $|\omega_s - \omega_t|$ is a member of $[\omega_{\rm th1},\ \omega_{\rm th2})$, the two components are the twin components of beats,
3) otherwise, they are two distinct components of a modal oscillation.

To this end, $\omega_{\rm th1}$ can be typically chosen as half of the resonant peak width $\zeta_r\omega_{\rm nr}$ (see Fig. 1). In the remainder of this section, a practical method for determining $\omega_{\rm th2}$ is presented. The critical of this method is to derive the upper bound of $|\omega_{\rm dr} - \omega_l|$. To achieve this, a proposition is given at first.

Proposition 1: For beats, a basic relationship is actually underlaid the waveforms, i.e., the difference between $\omega_{\rm dr}$ and ω_l should be less than either of the frequencies. Mathematically, it can be expressed as:

$$|\omega_{\rm dr} - \omega_l| < \min(\omega_{\rm dr},\ \omega_l). \tag{17}$$

Proof: Equation (17) can be expanded to two cases, i.e.,

$$\begin{cases} \dfrac{\omega_{\rm dr}}{\omega_l} \in (1,\ 2) & \text{if } \omega_{\rm dr} > \omega_l, \\ \dfrac{\omega_l}{\omega_{\rm dr}} \in (1,\ 2) & \text{if } \omega_{\rm dr} < \omega_l. \end{cases} \tag{18}$$

Define averages of the sum and absolute difference of $\omega_{\rm dr}$ and ω_l respectively as:

$$\omega_{\rm ar} = \frac{\omega_{\rm dr} + \omega_l}{2},\ \omega_{\rm br} = \frac{|\omega_{\rm dr} - \omega_l|}{2}. \tag{19}$$

By taking (18) into account, the ratio of $\omega_{\rm ar}$ to $\omega_{\rm br}$ is analyzed as follows.

$$\frac{\omega_{\rm ar}}{\omega_{\rm br}} = \begin{cases} \dfrac{\omega_{\rm dr} + \omega_l}{\omega_{\rm dr} - \omega_l} = 1 + \dfrac{2}{\omega_{\rm dr}/\omega_l - 1} > 3 & \text{if } \omega_{\rm dr} > \omega_l, \\ \dfrac{\omega_{\rm dr} + \omega_l}{\omega_l - \omega_{\rm dr}} = 1 + \dfrac{2}{\omega_l\omega_{\rm dr} - 1} > 3 & \text{if } \omega_{\rm dr} < \omega_l. \end{cases} \tag{20}$$

The physical meaning of (20) is that for beat frequency oscillation, there should be at least 3 peaks (or troughs) enclosed in one beat. As an extreme case, when $\omega_{\rm dr} = \omega_l$, resonance occurs and it contains an infinite number of peaks and troughs. These two conclusions can be verified from illustrative diagrams of beats and resonance, as shown in Figs. 3 and 4. □

From (18), we have:

$$\begin{cases} \dfrac{\omega_{\rm dr}}{\omega_l} < 2 \Rightarrow \dfrac{\omega_{\rm dr}}{2} < \omega_l \Rightarrow \omega_{\rm dr} - \omega_l < \dfrac{\omega_{\rm dr}}{2} & \text{if } \omega_{\rm dr} > \omega_l, \\ \dfrac{\omega_l}{\omega_{\rm dr}} < 2 \Rightarrow \dfrac{\omega_l}{2} < \omega_{\rm dr} \Rightarrow \omega_l - \omega_{\rm dr} < \dfrac{\omega_l}{2} & \text{if } \omega_{\rm dr} < \omega_l. \end{cases} \tag{21}$$

Combining the two cases in (21) yields the upper bound of $|\omega_{\rm dr} - \omega_l|$, i.e.,

$$|\omega_{\rm dr} - \omega_l| < \max\left(\frac{\omega_{\rm dr}}{2},\ \frac{\omega_l}{2}\right) = 1.0 \text{ Hz or } 2\pi \text{ rad/s}. \tag{22}$$

Equation (22) works for $\omega_{\rm dr},\ \omega_l \in [0.1,\ 2.0]$ Hz. Based on the equation, the threshold $\omega_{\rm th2}$ can be determined. In this paper, a relatively tight condition for detecting beats is used by setting $\omega_{\rm th2}$ as 0.2 Hz. Notice that it is consistent with the setting in [28].

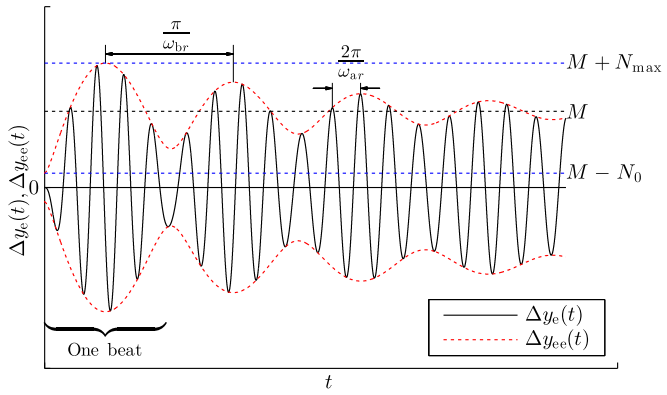

Fig. 3. Illustrative diagram of positive damping beats with $\omega_l < \omega_{\rm nr}$, $\beta > 1$ and $M > N_0$. $\Delta y_{\rm e}(t)$ is the waveform of beats and $\Delta y_{\rm ee}(t)$ is its upper or lower envelope. M, N_0 and $N_{\max}$ are defined and evaluated in (24), (25) and (30), respectively.

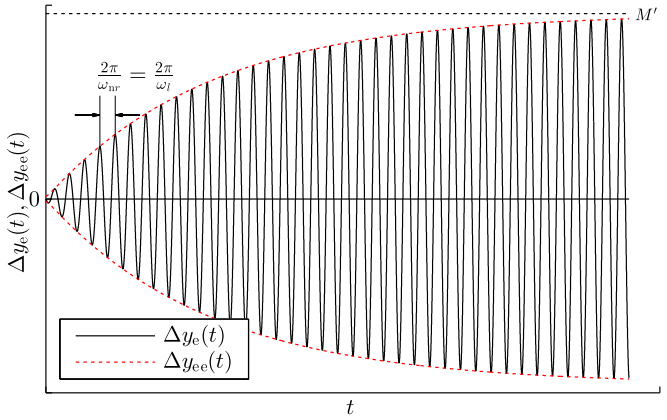

Fig. 4. Illustrative diagram of positive damping resonance. $\Delta y_{\rm e}(t)$ is the waveform of resonance and $\Delta y_{\rm ee}(t)$ is its upper or lower envelope. M' is defined in (37).

V. Forced Oscillation Envelope-Analysis and Detection

This section explores the envelope of forced oscillation. Based on uniqueness of envelope shapes, forced oscillation can be detected and distinguished from modal oscillation by visual inspection in the presence of single forced disturbance.

A. Envelope of Forced Oscillation

Equation (9) can be rewritten in a more compact form:

$$\Delta y(t) = \sum_{i=1}^{n}\sum_{r=1}^{q}\sum_{l=1}^{m}\big[-M\sin(\omega_l t+\gamma_{ir}+\alpha_{rl}-\varphi) + N\sin(\omega_{\rm dr}t+\gamma_{ir}+\alpha_{rl}-\varphi)\big] \tag{23}$$

by introducing amplitude constant M and variable N

$$M = \frac{2\omega_l c_i|\phi_{ir}||\psi_{rl}|\Delta P_l}{\eta}\beta \tag{24}$$

$$N(t) = \frac{2\omega_l c_i|\phi_{ir}||\psi_{rl}|\Delta P_l}{\eta}e^{-\zeta_r\omega_{\rm nr}t}. \tag{25}$$

Substituting $\omega_{\rm dr}$ and ω_l in (23) with $\omega_{\rm ar}+\omega_{\rm br}$ and $\omega_{\rm ar}-\omega_{\rm br}$, respectively, results in a reformulation of Δy.

$$\begin{aligned}\Delta y(t) &= \sum_{i=1}^{n}\sum_{r=1}^{q}\sum_{l=1}^{m}\Delta y_{1\rm e}(t)\cos(\omega_{\rm ar}t)+\Delta y_{2\rm e}(t)\sin(\omega_{\rm ar}t)\\ &= \sum_{i=1}^{n}\sum_{r=1}^{q}\sum_{l=1}^{m}\Delta y_{\rm e}(t)\end{aligned} \tag{26}$$

where

$$\begin{aligned}\Delta y_{1\rm e}(t) =\ & M\sin(\omega_{\rm br}t-\gamma_{ir}-\alpha_{rl}+\varphi)\\ &+N\sin(\omega_{\rm br}t+\gamma_{ir}+\alpha_{rl}-\varphi)\end{aligned} \tag{27}$$

$$\begin{aligned}\Delta y_{2\rm e}(t) =\ & -M\cos(\omega_{\rm br}t-\gamma_{ir}-\alpha_{rl}+\varphi)\\ &+N\cos(\omega_{\rm br}t+\gamma_{ir}+\alpha_{rl}-\varphi).\end{aligned} \tag{28}$$

Accordingly, the envelope that modulates the amplitude of $\Delta y_{\rm e}(t)$ can be obtained

$$\begin{aligned}\Delta y_{\rm ee}(t) &= \pm\sqrt{\Delta y_{1\rm e}^2(t)+\Delta y_{2\rm e}^2(t)}\\ &= \pm\sqrt{M^2+N^2-2MN\cos(2\omega_{\rm br}t)}.\end{aligned} \tag{29}$$

In the following sections, $\Delta y_{\rm e}(t)$ and $\Delta y_{\rm ee}(t)$ induced by a single forced disturbance are detailed in the cases of beats and resonance.

B. Envelope of Beats

In weakly damped and non-resonant operating condition, the third term under the square root sign in (29) is nonzero. It means that the amplitude of forced oscillation will vary or oscillate at a frequency of $2\omega_{\rm br}$, i.e., *beat frequency*.

It can be seen from Fig. 3 that there exist overshoots in the upper envelope. It attains the minimum and maximum values at $t=0$ and $\frac{\pi}{2\omega_{\rm br}}$, i.e., $|M-N_0|$ and $|M+N_{\max}|$, where

$$N_0 = N(0),\ N_{\max} = N\Big(\frac{\pi}{2\omega_{\rm br}}\Big). \tag{30}$$

In the following, two special cases of beats are considered:

1) Beats arrive in steady state and N tends to $N(\infty)=0$.
2) In the absence of damping, undamped beats occur.

In the first case, $\Delta y_{\rm ee}(t)$ is a constant and $\Delta y_{\rm e}(t)$ becomes an undamped oscillation, i.e.,

$$\Delta y_{\rm e}(t) = \Delta y_{\rm ee}\cdot\sin(\omega_l t+\gamma_{ir}+\alpha_{rl}-\varphi) \tag{31}$$

$$\Delta y_{\rm ee} = \pm M. \tag{32}$$

In the second case, $\zeta_r=0$, $\varphi=\frac{\pi}{2}$. $\Delta y_{\rm ee}(t)$ is an undamped oscillation and $\Delta y_{\rm e}(t)$ becomes undamped beats, viz.,

$$\begin{aligned}\Delta y_{\rm e}(t) =\ & \frac{c_i|\phi_{ir}||\psi_{rl}|\Delta P_l}{2\omega_{\rm br}}\\ &\times\big[(\beta+1)\sin(\omega_{\rm br}t)\sin(\omega_{\rm ar}t+\gamma_{ir}+\alpha_{rl})\\ &-(\beta-1)\cos(\omega_{\rm br}t)\cos(\omega_{\rm ar}t+\gamma_{ir}+\alpha_{rl})\big]\end{aligned} \tag{33}$$

$$\Delta y_{\rm ee}(t) = \frac{c_i|\phi_{ir}||\psi_{rl}|\Delta P_l}{2\omega_{\rm br}}\sqrt{\beta^2+1-2\beta\cos(2\omega_{\rm br}t)}. \tag{34}$$

C. Envelope of Resonance

As a special case of beats, when resonance occurs, quantities in (11)–(13) can be reduced to $\eta = 2\zeta_r\omega_{\rm nr}\omega_l$, $\beta = 1$ and $\varphi = 0$, respectively. Considering $\omega_{\rm br} \approx 0$ and $\omega_{\rm ar} \approx \omega_{\rm nr} = \omega_l$, it can be known from (23) and (29) that

$$\begin{aligned}\Delta y_{\rm e}(t) = \; & \frac{c_i|\phi_{ir}||\psi_{rl}|\Delta P_l}{\zeta_r\omega_{\rm nr}} \\ & \times\big[\big(1+e^{-\zeta_r\omega_{\rm nr}t}\big)\sin(\omega_{\rm br}t)\cos(\omega_{\rm ar}t+\gamma_{ir}+\alpha_{rl}) \\ & -\big(1-e^{-\zeta_r\omega_{\rm nr}t}\big)\cos(\omega_{\rm br}t)\sin(\omega_{\rm ar}t+\gamma_{ir}+\alpha_{rl})\big] \\ \approx \; & \sum_{i=1}^{n}\sum_{r=1}^{q}\sum_{l=1}^{m}\Delta y_{\rm ee}(t)\sin(\omega_{\rm ar}t+\gamma_{ir}+\alpha_{rl}) \quad (35)\end{aligned}$$

$$\Delta y_{\rm ee}(t) = \; M - N = \pm\frac{c_i|\phi_{ir}||\psi_{rl}|\Delta P_l}{\zeta_r\omega_{\rm nr}}\big(e^{-\zeta_r\omega_{\rm nr}t}-1\big). \quad (36)$$

It can be seen from Fig. 4 that $\Delta y_{\rm ee}(t)$ is non-oscillatory and does not have any overshoot. Particularly, when resonance reaches steady state, $\Delta y_{\rm ee}(t)$ becomes a constant:

$$\Delta y_{\rm ee} = \; M' = \pm\frac{c_i\phi_{ir}\psi_{rl}\Delta P_l}{\zeta_r\omega_{\rm nr}}. \quad (37)$$

Note that here M' is much greater than M given in (32) / (24).

In the case of zero damping, the envelope of resonance can be obtained in two ways. On one hand, it is known that $\omega_{\rm br}t$ and $\sin(\omega_{\rm br}t)$ become two infinitesimals of the same order of magnitudes as $\omega_{\rm br}$ approaches zero. Accordingly, the envelope of zero damping resonance can be derived from the limit of (34) by making $\beta = 1$ and $\omega_{\rm br} \to 0$:

$$\Delta y_{\rm ee}(t) = \pm c_i\phi_{ir}\psi_{rl}\Delta P_l \cdot t. \quad (38)$$

On the other hand, the envelope can also be obtained by taking limit of (36) and considering the fact that $e^{-\zeta_r\omega_{\rm nr}t}-1$ and $-\zeta_r\omega_{\rm nr}t$ are two infinitesimals of the same order of magnitudes when ζ_r is sufficiently close to zero.

As it is seen from (38) that the envelope of zero damping resonance grows linearly with time t. Without taking any remedial measures, the oscillation will grow unlimitedly. Ultimately, the system will experience a catastrophic blackout.

D. Envelope-Shape-Analysis-Based Forced Oscillation Detection

Mathematically, the shapes of envelopes can be determined by signs of their first and second time derivatives, as summarized in columns 4–7 of Table I.

Intuitively, the envelops of beats in Cases 1 and 2 are undamped and damped oscillations, respectively, corresponding to their zero-crossing time derivatives. Case 3 shows that the envelope of zero damping resonance is an oblique line. Case 4 implies a convex upper envelope of positive damping resonance.

Compared with forced oscillations, Cases 6 and 7 denote that upper envelopes of modal oscillations are concave for the system in both positive and negative damping conditions. For the zero damping modal oscillation, its envelope is a horizontal line, as given by Case 5.

TABLE I
UPPER ENVELOPE SHAPES OF FORCED AND MODAL OSCILLATIONS

Oscillation Type		Case No.	ζ_r	$\Delta y'_{\rm ee}$	$\Delta y''_{\rm ee}$	$\Delta y'_{\rm ee} * \Delta y''_{\rm ee}$	Envelope Shape
Forced oscillation	Beats	1	$=0$	$\pm,0$	$\pm,0$	$\pm,0$	Undamped oscillation
		2	>0	$\pm,0$	$\pm,0$	$\pm,0$	Damped oscillation
	Resonance	3	$=0$	$+$	0	0	Oblique line
		4	>0	$+$	$-$	$-$	Convex
		5	$=0$	0	0	0	Horizontal line
Modal oscillation		6	>0	$-$	$-$	$+$	Concave and growing
		7	<0	$+$	$+$	$+$	Concave and decaying

Therefore, by keeping the uniqueness of envelope shapes (see column 7 of Table I) in mind and visually inspecting their transient responses, forced and modal oscillations can be easily detected and discriminated from each other.

E. Discussion

The component-analysis-based forced oscillation detection method is capable of detecting forced oscillation in case of multiple forced disturbances. It can even deal with the mixture of forced and modal oscillations.

Compared with component-analysis-based forced oscillation detection method, the envelope-shape-based method is intuitive. However, the latter is of more theoretical value because it cannot handle complex waveforms of oscillations in the circumstances of multiple forced disturbances. For the realistic case, neither do we know the number of forced oscillation sources in the system nor their nature (i.e., resonance or beats) beforehand. Furthermore, for oscillations occurred in practical power system, the captured signals contain non-oscillatory component and ambient noises. Because the envelope shapes of forced oscillations are distorted from the ideal ones to some extent, the component-analysis-based method is then preferred for the reliable detection of forced oscillation.

VI. Case Study I: Forced Oscillations in the New England Test System

The 10-machine 39-bus New England test system as depicted in Fig. 5 is employed to demonstrate the correctness of theoretical analyses and the effectiveness of detection methods for forced oscillation. Various cases in which the system is disturbed by single forced disturbance, two forced disturbances, and two forced disturbances plus an exciter step are intensively investigated.

A. Description of the Test System

Under normal operating condition, active power across tielines {16–15, 16–17} is 3.91 p.u.. Generators are represented by the two-axis model and equipped with IEEE type DC1A

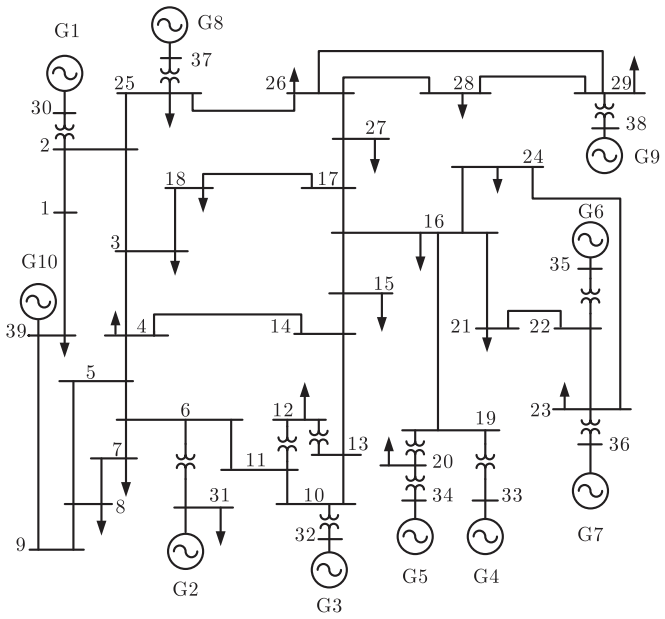

Fig. 5. One-line diagram of the 10-machine 39-bus New England test system.

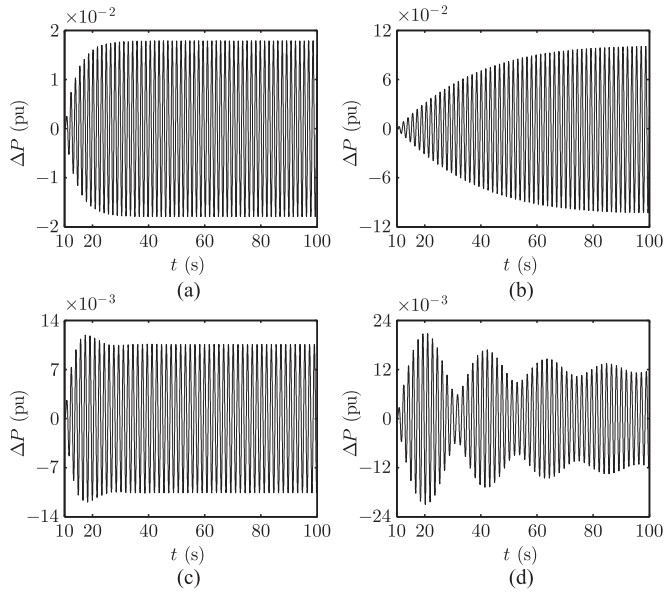

Fig. 6. Deviations of active power on tie-line 16–17 when the forced disturbance sits on G10. (a) Case 1: resonance under $\zeta_r = 5.32\%$; (b) Case 2: resonance under $\zeta_r = 0.38\%$; (c) Case 3: beats under $\zeta_r = 5.32\%$; (d) Case 4: beats under $\zeta_r = 0.38\%$.

excitation system. Loads are simulated by constant impedances. Detail parameters of the system can be found in [27].

Two scenarios of different damping levels of the inter-area mode, in which G10 oscillates against G1–G9, are built by adjusting the gains of exciters. In the well-damped Scenario 1, parameters of exciters are the same as those shown in [27]. Frequency and damping ratio of the mode are 0.637 Hz and 5.32%, respectively. In the poorly damped Scenario 2, gains of all exciters are replaced by a relatively high value of 40. Accordingly, frequency of the mode becomes 0.615 Hz and the damping ratio reduces to 0.38%.

B. Single Forced Disturbance

The forced disturbance is located on the dominant generator G10 and has a small magnitude of 0.02 p.u.. The perturbation is activated at $t = 10$ s. Four cases are studied. In Cases 1 and 2, frequencies of forced disturbances are set to the resonant frequencies in Scenarios 1 and 2. They can be computed from (8) and (15), viz., 0.638 and 0.615 Hz, respectively. In Cases 3 and 4, the disturbance frequencies are 0.05 Hz below the two resonant frequencies, i.e., 0.588 and 0.565 Hz, respectively. Accordingly, two beats are simulated. In all cases, deviations of active power on tie-line 16–17 are shown in Fig. 6(a)–(d), respectively.

First, forced oscillation amplitudes are analyzed. Compared with Cases 1 and 3 in Scenario 1, Cases 2 and 4 in Scenario 2 clearly show that longer time is needed to reach steady state due to smaller damping ratio of the inter-area mode. Besides, the steady state amplitude of resonance in Case 2 is six times of that in Case 1. For beats in Case 4, the maximum of the transient amplitude is twice as much as that in Case 3. However, their steady state amplitudes are nearly the same since they are mainly determined by the same frequency differences between forced disturbance and system mode, i.e., 0.05 Hz. Additionally, it is apparent that the steady state amplitudes of resonances are greater than those of beats. Specifically, in Scenario 1, the amplitude in Case 1 is almost 1.8 times as much as that in Case 3. While in the poorly damped Scenario 2, the amplitude ratio of Case 2 to Case 4 exceeds 8.

TABLE II
PRONY ANALYSIS FOR SYSTEM DISTURBED BY SINGLE FORCED DISTURBANCE

Case No.	Component No.	Amplitude	Frequency (Hz)	Phase (deg.)	Damping Ratio (%)
1	1	0.0089	0.6380	178.35	−0.0003
	2	0.0091	0.6391	−4.54	5.6574
2	1	0.0492	0.6145	171.39	−0.0074
	2	0.0545	0.6145	−13.72	1.2685
3	1	0.0053	0.5880	−125.68	−0.0011
	2	0.0050	0.6394	50.04	5.3874
4	1	0.0061	0.5650	−87.18	−0.0001
	2	0.0059	0.6116	91.18	0.7573

Second, forced oscillation component analysis is carried out. The well-known Prony algorithm [37] is employed to extract oscillation components and simultaneously estimate system modes and forced oscillations from deviations of active power on the tie-line 16–17. The sample frequency is 20 Hz. For resonances and beats in Cases 1–4, their component quantities, frequencies and damping ratios are listed in Table II. In each case, two components with approximately the same amplitudes but almost in antiphase are identified. The damping ratio of the forced component is close to zero and its frequency is near that of the forced disturbance. The damping ratio and frequency of the free component are very close to those of the system mode. In summary, these findings are in well accordance with the

theoretical analyses for forced oscillation components presented in Section IV. Therefore, based on unique component properties of resonance and beats, they can be easily distinguished from each other.

Next, the envelope shapes of forced oscillations are inspected. For resonances in Cases 1 and 2, their upper envelopes are convex without any overshoot. For beats in Case 3, since the free component dies out rapidly, the overshoots in the envelope are very small and the beats are negligible. In the poorly damped Case 4, the oscillatory feature of envelopes is comparatively impressive. Therefore, it can be claimed that resonances and beats can be easily discriminated from each other according to their unique envelope shapes.

Based on above analyses, it should be emphasized that, in the case of single forced source disturbs the multimachine power system, both component-analysis and envelope-shape-analysis based method can accurately discriminate different types of forced oscillations.

C. Two Forced Disturbances

In Scenario 2, another local mode is selected via modal analysis so that the location and frequency of the second forced disturbance can be determined. The analysis reveals that G6 and G7 oscillate against G1, G5 and G8 at a frequency of 1.13 Hz and with a damping ratio of 1.74%. To sufficiently excite the mode, this forced disturbance sits on the dominant generator G6. Its magnitude is set as 0.02 p.u..

Another three cases are then studied. In Case 5, frequencies of the two forced disturbances are identical to natural frequencies of the inter-area and local modes, respectively, viz., 0.615 and 1.13 Hz, resulting in two resonances in the forced oscillation. Subsequently, in Case 6, the frequency of the first forced disturbance on G10 is changed to 0.02 Hz below the resonant frequency, i.e., 0.595 Hz. It is clear the resultant forced oscillation is a hybrid of beats and resonance. Lastly, in Case 7, both the frequencies of the two forced disturbances are set to be 0.02 Hz below the resonant frequencies, i.e., 0.595 and 1.11 Hz, respectively. Accordingly, two beats occur.

The active power deviations on the tie-line 16–17 in Cases 5–7 are shown in Fig. 7(a)–(c), respectively. Notice that the waveforms of the forced oscillations are more complex, compared with those in Fig. 6 where the system is disturbed by only one source. Taking Fig. 7(a) as an example, it can be seen that the synthesis of two resonances present as beats. Therefore, the component-analysis-based method is utilized to confirm these forced oscillations.

Similar to the single forced disturbance case, again, the estimation results listed in Table III show that the Prony algorithm can estimate both system modes and forced oscillations in all three cases. In each case, two pairs of free and forced oscillation components are caused by the two forced disturbances.

D. Two Forced Disturbances and an Exciter Step

This section further investigates the capability of the component-analysis-based method in detecting forced oscillation when both forced and modal oscillations are simultaneously presented in the system.

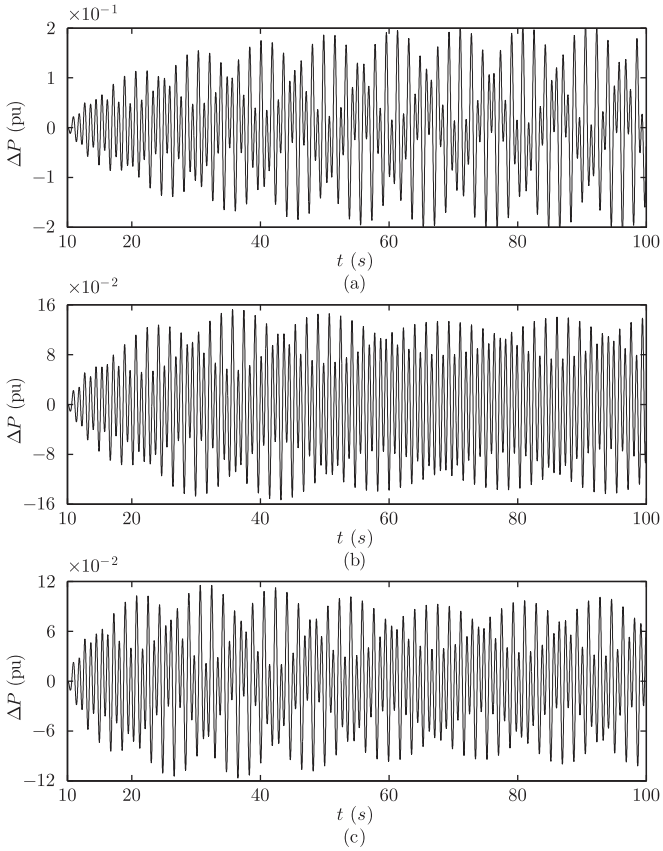

Fig. 7. Deviation of active power on tie-line 16–17 when two forced disturbances are located on G10 and G6 in Scenario 2. (a) Case 5: two resonances; (b) Case 6: hybrid of beats and resonance; (c) Case 7: two beats.

TABLE III
PRONY ANALYSIS FOR SYSTEM DISTURBED BY TWO FORCED DISTURBANCES

Case No.	Component No.	Amplitude	Frequency (Hz)	Phase (deg.)	Damping Ratio (%)
5	1	0.0491	0.6150	149.87	0.0003
	2	0.0485	0.6114	−29.04	0.7594
	3	0.0536	1.1300	−8.35	0.0007
	4	0.0538	1.1296	−173.43	1.8774
6	1	0.0168	0.5950	−97.51	−0.0005
	2	0.0179	0.6114	83.25	0.7613
	3	0.0535	1.1300	−8.17	0.0005
	4	0.0525	1.1308	−177.28	1.8861
7	1	0.0168	0.5950	−97.51	−0.0002
	2	0.0180	0.6114	83.29	0.7628
	3	0.0326	1.1100	26.37	−0.0010
	4	0.0368	1.1302	−132.76	1.8511

To this end, besides the forced disturbances in Cases 5–7, an extra exciter steps with 3% magnitude change is applied to generator G6 to excite modal oscillation in each case. Accordingly, another three Cases 8–9 are obtained. The active power deviations on the tie-line 16–17 in all cases are analyzed by the Prony algorithm. The estimated oscillations components and their oscillatory properties are listed in Table IV.

TABLE IV
PRONY ANALYSIS FOR SYSTEM DISTURBED BY TWO FORCED DISTURBANCES AND A 3% EXCITER STEP

Case No.	Component No.	Amplitude	Frequency (Hz)	Phase (deg.)	Damping Ratio (%)
8	1	0.0438	0.6150	170.52	−0.0091
	2	0.0416	0.6129	−20.64	1.0570
	3	0.0543	1.1300	−1.08	0.0008
	4	0.0578	1.1329	−167.89	1.8303
9	1	0.0151	0.5950	−100.63	−0.0015
	2	0.0078	0.6129	106.16	1.0176
	3	0.0541	1.1300	−1.33	0.0001
	4	0.0620	1.1335	−173.05	1.9673
10	1	0.0119	0.5950	75.97	−0.0021
	2	0.0062	0.6129	−77.21	1.0210
	3	0.0117	1.1100	−164.21	0.0003
	4	0.0176	1.1335	47.36	1.9669

It can be seen from the table that, in each case, two pairs of free and forced oscillation components can be accurately and reliably identified. The estimation results validate the capability of the presented component-analysis-based method in detecting forced oscillations in cases where both forced and modal oscillations are involved in the system.

The estimation results in Table IV are then compared with those in Table III. It can be found that amplitudes of the free components for beats, i.e., component 2 in Case 9, components 2 and 4 in Case 10, are largely weakened by the newly introduced modal oscillation due to possible anti-phase. Furthermore, since the amplitudes of resonances in Cases 8 and 9 are much greater than those of the modal oscillations, they are basically unaffected by the exciter step.

VII. CASE STUDY II: FORCED OSCILLATION IN A REAL-LIFE POWER SYSTEM

In this section, an active power oscillation occurred in Shandong power system of China on June 18, 2012 is analyzed to demonstrate the correctness of the component-analysis-based method for detecting forced oscillation. Further, possible causes of the oscillation are provided.

A. Description of the Oscillation

The oscillation occurred at the 670 MW tandem compound, 3000 rpm turbine-generator unit #5 in WH power plant. During the event, active power output of the generator was captured by the wide-area measurement system (WAMS), as shown in Fig. 8.

Prior to experiencing the oscillation, the generator was operated at its rated active power. From local time 17:09:51, the power order (load reference) of the unit began to fluctuate and active power generation oscillated accordingly. The peak-to-peak amplitude of the oscillation was approximately 120 MW and the frequency was about 1.0 Hz. Four more oscillations recurred on June 18 (once), 21 (twice) and 22 (once) when the unit was operated at full load.

These oscillations could always decay by switching the digital electro-hydraulic governing system (DEH) of the unit from coordinated control (CC) mode to boiler input (BI, i.e., turbine following the boiler) control mode [38], [39].

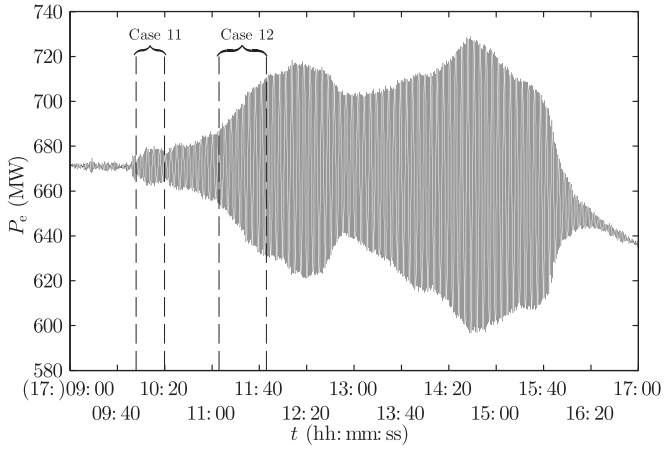

Fig. 8. Active power output of unit #5 in WH power plant during the oscillation event.

TABLE V
PRONY ANALYSIS OF THE ACTIVE POWER GENERATION

Case No.	Component No.	Amplitude	Frequency (Hz)	Phase (deg.)	Damping Ratio (%)
11	1	3.9837	0.9824	57.34	0.0624
	2	4.5537	0.9984	−145.74	6.0993
	3	0.4616	1.3184	−44.21	4.8489
	4	0.1426	1.4356	157.21	22.3679
	5	0.1969	2.4255	124.80	14.3171
12	1	0.3909	0.6835	13.89	52.4161
	2	2.3857	0.9765	−134.43	7.3395
	3	9.3272	0.9892	4.62	−0.3288
	4	0.5729	1.9692	−65.65	8.6085
	5	0.4384	2.3186	19.58	20.1382

B. Oscillation Component Analysis

To reduce the adverse effect of nonlinearity, active power outputs of the unit at the early stage of the oscillation, viz., 17:09:56-17:10:20 (24 s, Case 11) and 17:11:06-17:11:46 (40 s, Case 12) are down-sampled at a frequency of 25 Hz for Prony analyses. The first five oscillatory components with the lowest frequencies are listed in Table V.

As can be seen from the table, the components 1 and 2 in Case 11 have extremely larger amplitudes than the remaining. In addition, the frequencies of the two components are very close. The damping ratio of component 1 is determined as zero and that of component 2 is greater than zero. The frequencies of components 1 and 2 are nearly the same. Furthermore, the same findings are obtained by analyzing the dominant components 2 and 3 in Case 12.

By using the component-analysis-based method presented in Section IV-B, it can be claimed that the oscillation belongs to forced oscillation. To be more exact, it is resonance.

C. Possible Causes of the Oscillations

Up to the present, the exact causes of the successive five forced oscillations are still unknown for two reasons. On one hand, unlike WAMS, the sampling period of DEH of the unit is relatively large (i.e., 0.2 s), resulting in an absence of high-precision data required for joint thermal and electrical analyses. On the other hand, oscillations did not recur in subsequent routine operation and filed tests. However, an attempted explanation for possible causes of the oscillations is provided as follows, based on post-incident analyses, field tests and practical remedial actions for the unit. To some extent, these analyses and tests support the assertion based on oscillation component analysis as addressed in the last section.

First, the eigen-analysis revealed that the unit only dominated a well-damped plant mode, whose frequency and damping ratio were 0.988 Hz and 8.53%, respectively. They coincide with the free component 2 in both Cases 11 and 12, as shown in Table V. Thus, the practical oscillations were indeed forced oscillations rather than modal oscillations with negative damping. Second, exciter step response tests with 3% magnitude change were performed at different load levels, with or without PSSs. Satisfactory damping of system responses in all cases excluded the possibility of exciter and PSS being the oscillation sources. Furthermore, it was observed that identical emergency controls were carried out after the five forced oscillations, i.e., switching the control mode of the governing system from CC to BI. Therefore, it is highly likely that the governing system amplified some possible disturbance sources (e.g., the high penetration of wind power in WH region) and caused the oscillations.

To reduce the over-sensitivity of governing system to external load variations, two remedial actions were taken. First, an inertial block (i.e., a low-pass filter) with a time constant of 2 s was added in front of the active power measuring module of the DEH. Second, both the proportional and integral gains of the governor's PID controller were slightly reduced. At this time, the unit is able to operate at full load while the system is stabilized and forced oscillations do not recur. However, one cannot claim that the forced oscillations are thoroughly suppressed by these remedial actions because the external forced disturbances may be temporary in nature and have completely vanished.

Therefore, pursuit for the exact causes of these forced oscillations is part of our future work, including reproduction of the recorded system response [1] and theoretical analysis by using other mechanisms of power system oscillation, e.g., strong modal resonance [40].

VIII. Conclusion

This paper theoretically analyzes the explicit expression, amplitude, components and envelope of forced oscillation in multimachine power system. Important conclusions are:

1) Higher observability/controllability, smaller damping ratio of system mode, and closer proximity of frequencies between forced disturbance and system mode, will result in strong forced oscillation.
2) Forced oscillation can be alleviated by reducing the amplitude of forced disturbance, eliminating its source, increasing the frequency difference between forced disturbance and system mode, and improving system damping.
3) A forced disturbance leads to twin oscillation components. The forced one is zero damping and of the same frequency as forced disturbance. The free one is with the identical modal properties as system mode.
4) Envelope shapes of forced oscillations are unique. The upper envelope of resonance is non-oscillatory and can be distinguished from modal oscillation by its convexity. In comparison, the envelope of beats is always oscillatory.

Based on uniqueness of components properties and envelope shapes, forced oscillation can be reliably detected and correctly discriminated from modal oscillation.

References

[1] D. N. Kosterev, C. W. Taylor, and W. A. Mittelstadt, "Model validation for the August10, 1996 WSCC system outage," *IEEE Trans. Power Syst.*, vol. 14, no. 3, pp. 967–979, Aug. 1999.

[2] M. A. Magdy and F. Coowar, "Frequency domain analysis of power system forced oscillations," *IEE Proc-C Gen. Transm. Distrib.*, vol. 137, no. 4, pp. 261–268, Jul.1990.

[3] C. D. Vournas, N. Krassas, and B. C. Papadias, "Analysis of forced oscillations in a multimachine power system," in *Proc. Int. Conf. Control*, Mar. 1991, pp. 443–448.

[4] L. Vanfretti *et al.*, "Application of ambient analysis techniques for the estimation of electromechanical oscillations from measured PMU data in four different power systems," *Eur. Trans. Electr. Power*, vol. 21, no. 4, pp. 1640–1656, May 2011.

[5] J. E. Van Ness, "Response of large power systems to cyclic load variations," *IEEE Trans. Power App. Syst.*, vol. PAS-85, no. 7, pp. 723–727, Jul.1966.

[6] J. A. Pinneilo and J. E. Van Ness, "Dynamic response of a large power system to a cyclic load produced by a nuclear accelerator," *IEEE Trans. Power App. Syst.*, vol. PAS-90, no. 4, pp. 1856–1862, Jul.1971.

[7] K. R. Rao and L. Jenkins, "Studies on power systems that subjected to cyclic loads," *IEEE Trans. Power Syst.*, vol. 3, no. 1, pp. 31–37, Feb. 1988.

[8] N. Rostamkolai, R. Piwko, and A. Matusik, "Evaluation of the impact of a large cyclic load on the LILCO power system using time simulation and frequency domain techniques," *IEEE Trans. Power Syst.*, vol. 9, no. 3, pp. 1411–1416, Aug. 1994.

[9] X. Wang, X. Li, and F. Li, "Analysis on oscillation in electro-hydraulic regulating system of steam turbine and fault diagnosis based on PSOBP," *Exp. Syst. Appl.*, vol. 37, no. 5, pp. 3887–3892, May 2010.

[10] J. O'Connor, V. Acharya, and T. Lieuwen, "Transverse combustion instabilities: Acoustic, fluid mechanic, and flame processes," *Prog. Energ. Combust. Sci.*, vol. 49, pp. 1–39, Aug. 2015.

[11] I. Hayashi and S. Kaneko, "Pressure pulsations in piping system excited by a centrifugal turbomachinery taking the damping characteristics into consideration," *J. Fluid. Struct.*, vol. 45, pp. 216–234, Feb. 2014.

[12] J. Hardin, F. Kushner, and S. Koester, "Elimination of flow-induced instability form steam turbine control valves," in *Proc. 32nd Turbomach. Symp.*, Sep. 2003, pp. 99–108.

[13] K. Yonezawa *et al.*, "Flow-induced vibration of a steam control valve," *J. Fluid. Struct.*, vol. 35, pp. 76–88, Nov. 2012.

[14] C. Bolin and A. Engeda, "Analysis of flow-induced instability in a redesigned steam control valve," *Appl. Therm. Eng.*, vol. 83, pp. 40–47, May 2015.

[15] D. S. L. Dolan and P. W. Lehn, "Simulation model of wind turbine 3p torque oscillations due to wind shear and tower shadow," *IEEE Trans. Energy Convers.*, vol. 21, no. 3, pp. 717–724, Sep. 2006.

[16] C. Su, W. Hu, Z. Chen, and Y. Hu, "Mitigation of power system oscillation caused by wind power fluctuation," *IET Renew. Power Gener.*, vol. 7, no. 6, pp. 639–651, Nov. 2013.

[17] T. J. Larsen and T. D. Hanson, "A method to avoid negative damped low frequent tower vibrations for a floating, pitch controlled wind turbine," *J. Phys.: Conf. Ser.*, vol. 75, Jul. 2007, Art. no. 012073.

[18] R. B. Myers and D. J. Trudnowski, "Effects of forced oscillations on spectral-based mode-shape estimation," in *Proc. IEEE Power Energy Soc. General Meet.*, Jul. 2013, pp. 1–6.

[19] J. Follum and J. W. Pierre, "Detection of periodic forced oscillations in power systems," *IEEE Trans. Power Syst.*, vol. 31, no. 3, pp. 2423–2433, May2016.
[20] N. Zhou and J. Dagle, "Initial results in using a self-coherence method for detecting sustained oscillations," *IEEE Trans. Power Syst.*, vol. 30, no. 1, pp. 522–530, Jan. 2015.
[21] N. Zhou, "A cross-coherence method for detecting oscillations," *IEEE Trans. Power Syst.*, vol. 31, no. 1, pp. 623–631, Jan. 2016.
[22] R. Xie and D. Trudnowski, "Distinguishing features of natural and forced oscillations," in *Proc. IEEE Power Energy Soc. General Meet.*, Jul. 2015, pp. 1–5.
[23] S. A. N. Sarmadi and V. Venkatasubramanian, "Inter-area resonance in power systems from forced oscillations," *IEEE Trans. Power Syst.*, vol. 31, no. 1, pp. 378–386, Jan. 2016.
[24] N. Martins, "Efficient eigenvalue and frequency response methods applied to power system small-signal stability studies," *IEEE Trans. Power Syst.*, vol. 1, no. 1, pp. 217–224, Feb. 1986.
[25] C. D. Meyer, *Matrix Analysis and Applied Linear Algebra*. Philadelphia, PA, USA: SIAM, 2001, Art. no. 609.
[26] P. Kundur, *Power System Stability and Control*. New York, NY, USA: McGraw-Hill, 1994.
[27] G. Rogers, *Power System Oscillations*. Boston, MA, USA: Kluwer, 2000.
[28] L. Vanfretti, S. Bengtsson, V. S. Peric, and J. Gjerde, "Effects of forced oscillations in power system damping estimation," in *Proc. IEEE Int. Workshop Appl. Meas. Power Syst.*, Sept. 2012, pp. 1–6.
[29] K. C. Lee and K. P. Poon, "Analysis of power system dynamic oscillations with beat phenomenon by Fourier transformation," *IEEE Trans. Power Syst.*, vol. 5, no. 1, pp. 148–153, Feb. 1990.
[30] T. R. Nudell and A. Chakrabortty, "A graph-theoretic algorithm for localization of forced harmonic oscillation inputs in power system networks," in *Proc. Amer. Control Conf.*, Jun. 2014, pp. 1334–1340.
[31] J. Ma, P. Zhang, H. Fu, B. Bo, and Z. Y. Dong, "Application of phasor measurement unit on locating disturbance source for low-frequency oscillation," *IEEE Trans. Smart Grid*, vol. 1, no. 3, pp. 340–346, Dec. 2010.
[32] Y. Li, C. Shen, and F. Liu, "An energy-based methodology for locating the source of forced oscillations in power systems," in *Proc. IEEE Int. Conf. Power Syst. Tech.*, Oct.-Nov. 2012, pp. 1–6.
[33] L. Chen, Y. Min, and W. Hu, "An energy-based method for location of power system oscillation source," *IEEE Trans. Power Syst.*, vol. 28, no. 2, pp. 828–836, May 2013.
[34] J. E. Van Ness, F. M. Brasch, G. L. Landgren, and S. T. Naumann, "Analytical investigation of dynamic instability occurring at Powerton station," *IEEE Trans. Power App. Syst.*, vol. PAS-99, no. 4, pp. 1386–1395, Jul./Aug. 1980.
[35] C. Y. Chung, L. Wang, F. Howell, and P. Kundur, "Generation rescheduling methods to improve power transfer capability constrained by small-signal stability," *IEEE Trans. Power Syst.*, vol. 19, no. 1, pp. 524–530, Feb. 2004.
[36] S. A. Nezam Sarmadi and V. Venkatasubramanian, "Electromechanical mode estimation using recursive adaptive stochastic subspace identification," *IEEE Trans. Power Syst.*, vol. 29, no. 1, pp. 349–358, Jan. 2014.
[37] J. F. Hauer, C. J. Demeure, and L. L. Scharf, "Initial results in Prony analysis of power system response signals," *IEEE Trans. Power Syst.*, vol. 5, no. 1, pp. 80–89, Feb. 1990.
[38] "Dynamic models for fossil fueled steam units in power system studies," *IEEE Trans. Power Syst.*, vol. 6, no. 2, pp. 753–761, May 1991.
[39] D. Flynn, *Thermal Power Plant Simulation and Control*. London, U.K.: The IET, 2003, pp. 209–211.
[40] I. Dobson, J. Zhang, S. Greene, H. Engdahl, and P. W. Sauer, "Is strong modal resonance a precursor to power system oscillations?" *IEEE Trans. Circuit Syst.-I*, vol. 48, no. 3, pp. 340–349, Mar. 2001.

Hua Ye (M'13) received the B.Eng. and Ph.D. degrees in electrical engineering from Shandong University, Ji'nan, China, in 2003 and 2009, respectively.

He is currently an Associate Professor at the Key Laboratory of Power System Intelligent Dispatch and Control of Ministry of Education, Shandong University, Ji'nan, China. From 2014 to 2015, he was also a Visiting Scholar at the University of Connecticut, Storrs, CT, USA. His research interests include power system dynamic stability analysis and control, cyber-physical power system.

Yutian Liu (SM'96) received the B.Eng. and M.S. degrees in electrical engineering from Shandong University of Technology, Ji'nan, China, in 1984 and 1990, respectively, and the Ph.D. degree in electrical engineering from Xi'an Jiaotong University, Xi'an, China, in 1994.

He is currently a Professor at the Key Laboratory of Power System Intelligent Dispatch and Control of Ministry of Education, Shandong University, Ji'nan, China. His research interests include power system analysis and control and artificial intelligence applications in power systems.

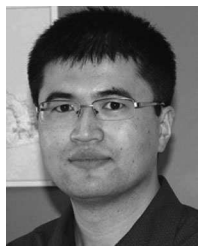

Peng Zhang (M'07-SM'10) received the Ph.D. degree in electrical engineering from the University of British Columbia, Vancouver, BC, Canada.

He is currently an Assistant Professor of electrical engineering at the University of Connecticut, Storrs, CT, USA. He was a System Planning Engineer at BC Hydro and Power Authority, Vancouver. His research interests include power system resilience and reliability, microgrid, distributed renewable energy systems, wide area measurement and control systems and active distribution grid.

He is a Registered Professional Engineer in British Columbia, Canada.

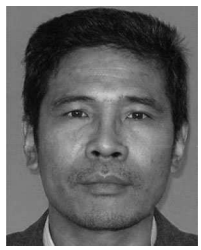

Zhengchun Du (M'12) received the B.S., M.S., and Ph.D. degrees in electrical engineering from Xi'an Jiaotong University, Xi'an, China, in 1983, 1986, and 1993, respectively.

He is currently a Professor of electrical engineering at Xi'an Jiaotong University, Xi'an, China. His research interests include power system stability analysis and control.